Title

Extensive Transduction and Enhanced Spread of a Modified AAV2 Capsid in the Non-human Primate CNS

Journal

Molecular Therapy, 26(10)

ISSN

1525-0016

Authors

Naidoo, Jerusha
Stanek, Lisa M
Ohno, Kousaku
et al.

Publication Date

2018-10-01

DOI

10.1016/j.ymthe.2018.07.008

Peer reviewed

Molecular Therapy
Original Article

Extensive Transduction and Enhanced Spread of a Modified AAV2 Capsid in the Non-human Primate CNS

Jerusha Naidoo,[1] Lisa M. Stanek,[2,3] Kousaku Ohno,[1,3] Savanah Trewman,[1] Lluis Samaranch,[1] Piotr Hadaczek,[1] Catherine O'Riordan,[2] Jennifer Sullivan,[2] Waldy San Sebastian,[1] John R. Bringas,[1] Christopher Snieckus,[1] Amin Mahmoodi,[1] Amir Mahmoodi,[1] John Forsayeth,[1] Krystof S. Bankiewicz,[1] and Lamya S. Shihabuddin[2]

[1]Interventional Neuro Center, Department of Neurological Surgery, University of California, San Francisco, San Francisco, CA, USA; [2]CNS Genetic Diseases, Neuroscience Research TA, Sanofi, Framingham, MA, USA

The present study was designed to characterize transduction of non-human primate brain and spinal cord with a modified adeno-associated virus serotype 2, incapable of binding to the heparan sulfate proteoglycan receptor, referred to as AAV2-HBKO. AAV2-HBKO was infused into the thalamus, intracerebroventricularly or via a combination of both intracerebroventricular and thalamic delivery. Thalamic injection of this modified vector encoding GFP resulted in widespread CNS transduction that included neurons in deep cortical layers, deep cerebellar nuclei, several subcortical regions, and motor neuron transduction in the spinal cord indicative of robust bidirectional axonal transport. Intracerebroventricular delivery similarly resulted in widespread cortical transduction, with one striking distinction that oligodendrocytes within superficial layers of the cortex were the primary cell type transduced. Robust motor neuron transduction was also observed in all levels of the spinal cord. The combination of thalamic and intracerebroventricular delivery resulted in transduction of oligodendrocytes in superficial cortical layers and neurons in deeper cortical layers. Several subcortical regions were also transduced. Our data demonstrate that AAV2-HBKO is a powerful vector for the potential treatment of a wide number of neurological disorders, and highlight that delivery route can significantly impact cellular tropism and pattern of CNS transduction.

INTRODUCTION

Adeno-associated viral vector serotype 2 (AAV2) has long been favored for neurological applications because of its neuronal specificity, and numerous studies have demonstrated longevity of transgene expression and clinical safety.[1,2] Despite its advantages, AAV2 has not always translated well from preclinical studies to the clinic for CNS indications largely because of the limited spread and transduction efficiency in large target regions of the brain.[3,4] The incorporation of convection-enhanced delivery (CED), a technique that involves exerting positive pressure to the cannula tip causing bulk flow of macromolecules within brain parenchyma,[5,6] has significantly improved distribution of AAV vectors by enhancing the volume of distribution and creating more uniform drug concentration at the target site.[3,4,7] The function of specific AAV capsid proteins has also been extensively probed in a bid to enhance tissue distribution (reviewed in Bobo et al.,[5] Morrison et al.,[6] Grishagin,[8] and Kotterman and Schaffer[9]). Heparan sulfate proteoglycans (HSPGs) are one such protein. HSPG receptors were long considered the sole receptor for entry of AAV2 into neurons,[3,4,10,11] but recently other receptors have been identified.[5,6,12–15] HSPG and its membrane receptor are abundantly expressed in the brain, possibly to limit distribution of multiple functional proteins such as coagulation cofactors, chemokines, and growth factors,[3,4,7,16,17] and to focus biological activity to anatomically distinct regions. We have previously demonstrated that co-infusion of heparan with therapeutics including AAV2 enhances the area of distribution in the rat striatum likely through competitive blocking of binding sites.[5,6,8,9,18,19] These findings indicate that removal of HSPG binding capability by capsid mutagenesis may not be detrimental to entry of AAV2 into brain cells.

Given that AAV2 has proven extremely valuable for clinical applications, it is important to determine whether removal of the HSPG binding sites allows the vector to retain its ability to safely and efficiently transduce brain cells. Consistent with previous reports, we have found that ablation of heparan sulfate binding enhanced the ability of AAV2 to bind and transduce neurons in the rodent brain and increased the volumetric spread of the vector.[20–22] As highlighted by Wilson and colleagues,[23] AAV transduction patterns in rodents do not always correlate in larger mammals. Studies in larger mammalian brains are therefore critical to establish the potential clinical utility of an AAV2 variant that does not bind HSPGs.

Received 7 April 2018; accepted 3 July 2018;
https://doi.org/10.1016/j.ymthe.2018.07.008.

[3]These authors contributed equally to this work.

Correspondence: Krystof S. Bankiewicz, Interventional Neuro Center, Department of Neurological Surgery, University of California, San Francisco, UCSF Mission Center Building 0555, 1855 Folsom St., Room 226, San Francisco, CA 94103-0555, USA.
E-mail: krystof.bankiewicz@ucsf.edu

The primary goals of the present study were to: (1) evaluate the effect of HSPG receptor binding abrogation on vector distribution and tropism, (2) evaluate the effect of HSPG receptor binding abrogation on axonal transport properties of the vector, and (3) explore the effect of route of administration on vector distribution in the brain and spinal cord of non-human primates (NHPs). Our modified AAV2 vector, referred to as AAV2-HBKO, was evaluated in the NHP brain and spinal cord after either thalamic, intracerebroventricular (ICV), or a combination of both thalamic and ICV delivery. The results indicate that (1) AAV2-HBKO transduces neurons independent of HSPG receptor binding and maintains neuronal tropism following parenchymal delivery, (2) AAV2-HBKO undergoes extensive bidirectional axonal transport when injected into the parenchyma, and (3) the route of administration impacts cellular tropism of AAV2-HBKO. When injected into the thalamus, the vector distributed extensively and neuronal transduction exceeded that previously observed with the parent AAV2 vector.[1,16,24] Neuronal transduction was observed in deep layers of the cortex, deep cerebellar nuclei, and several subcortical regions indicative of robust bidirectional axonal transport. ICV delivery resulted in strong ependymal cell transduction in the ventricular zone, along with widespread cortical transduction. Strikingly, transduction was limited to superficial layers, and GFP expression was observed predominantly in oligodendrocytes. The combination of ICV and thalamic delivery resulted in robust transduction of a majority of cortical layers, with oligodendrocytes primarily transduced in layers 1–3 and neurons transduced in layers 4–6. Motor neuron transduction was observed in all levels of the spinal cord after thalamic delivery, ICV delivery, and the combination of both ICV and thalamic delivery. These findings highlight the potential clinical utility of heparan binding-deficient AAV2 vectors and have important implications for the treatment of neurological diseases requiring widespread and global distribution of gene therapy in the brain and spinal cord, such as motor neuron diseases and lysosomal storage disorders. Others have reported oligodendrocyte transduction in subcortical areas,[25] but this is the first demonstration of oligodendrocyte transduction in the NHP cortex by a modified AAV2 capsid. AAV2-HBKO has possible application for demyelinating diseases, leukodystrophies, and other myelin disorders.

RESULTS

Thalamic AAV2-HBKO Infusion Results in Bidirectional Axonal Transport, Widespread Neuronal Transduction in Deep Cortical Layers, and Spinal Cord Transduction

AAV2-HBKO was delivered under intraoperative MRI guidance bilaterally into the thalamus (n = 3; 1.6–3.4 $\times$ 10^{12} vector genomes [vg]/hemisphere). No adverse effects were observed during infusion in the vasculature or parenchyma. MRI and 3D reconstruction of gadolinium signal revealed that the vector remained primarily within the target site. A small amount of leakage occurred into the subthalamic nucleus (STN), but no infusate was seen in the neighboring putamen or other non-targeted structures (Figure 1A). Tissue analysis of the injection sites revealed that AAV2-HBKO vector carrying a foreign protein (EGFP) triggered an immune reaction after being infused into the parenchyma, a finding consistently observed with expression of EGFP into antigen-presenting cells in the brain.[26–28] H&E staining revealed perivascular cuffing and cellular infiltration in the thalamus, and to a lesser extent in the secondary transduction areas. Astrocytic activation and microglial hyperactivity were also evident from glial fibrillary acidic protein (GFAP) and Iba1 staining in the thalamus, indicating a clear immune reaction (Figure S1). Visual examination of neuronal nuclei (NeuN) staining showed that there was no noteworthy loss of neurons in the thalamus or cortex, and none of the animals presented any gross adverse clinical signs throughout the duration of the study. Thalamic injection of AAV2-HBKO elicited robust anterograde transport to the cortex, with transduction extending from the prefrontal cortex to areas of parietal and temporal cortex just above the brainstem (Figure 1B). Quantification of cortical transduction area revealed that of the total cortical area, 80% of the prefrontal and frontal cortex, 37% of the temporal and parietal cortex, and 14% of the occipital cortex were transduced. Transduced cells were limited to deep cortical layers 4–6 in NHP. Double-immunofluorescent labeling experiments, in which GFP expression was coupled with NeuN, as a marker for neurons, revealed that greater than 90% of transduced cells were neuronal (Figures 1C, 1D, 2A, and 2B).

In addition to anterograde axonal transport to the cortex, AAV2-HBKO underwent retrograde axonal transport to several subcortical regions. GFP staining was evident in the caudate and putamen, globus pallidus (GP), substantia nigra pars reticulata (SNr), substantia nigra pars compacta (SNc), and brainstem (Figure 1E; Table 1).

GFP staining revealed the presence of GFP-positive cells at all levels of the spinal cord (i.e., cervical, thoracic, lumbar, and sacral; Figure 3A) in both the dorsal and ventral horns and the intermediate zone. Double-immunofluorescent labeling with GFP and NeuN revealed that the transduced cells were neurons. Both motor neurons and interneurons were transduced in the ventral horn. Transduced motor neurons in the ventral horn were identified with GFP and NeuN double labeling and morphologically by their large cell bodies (Figure 3B). Quantification of the number of transduced motor neurons revealed 65% motor neuron transduction in the cervical spinal cord, and 33%, 38%, and 33% of motor neurons in the thoracic, lumbar, and sacral regions, respectively (Figure 3C).

ICV AAV2-HBKO Infusion Results in Widespread Oligodendrocyte Transduction in Superficial Cortical Layers and Robust Motor Neuron Transduction in the Spinal Cord

AAV2-HBKO was delivered bilaterally to the lateral ventricle (n = 3; 1.8 $\times$ 10^{13} vg/hemisphere) under MRI guidance. As with the thalamic infusions, we did not observe any adverse effects during infusion. MRI of gadolinium signal revealed that there was no vector leakage into surrounding parenchyma. AAV2-HBKO rapidly distributed through the ventricular system and central canal within 5 min of starting the infusion (Figure 4A). H&E staining revealed a slight increase in cellular infiltration and perivascular cuffing in the cortex. This region also showed signs of mild astrocytic activation and microglial hyperactivity, indicative of a mild immune response (Figure S2). Visual examination revealed that there was no loss of neurons in the

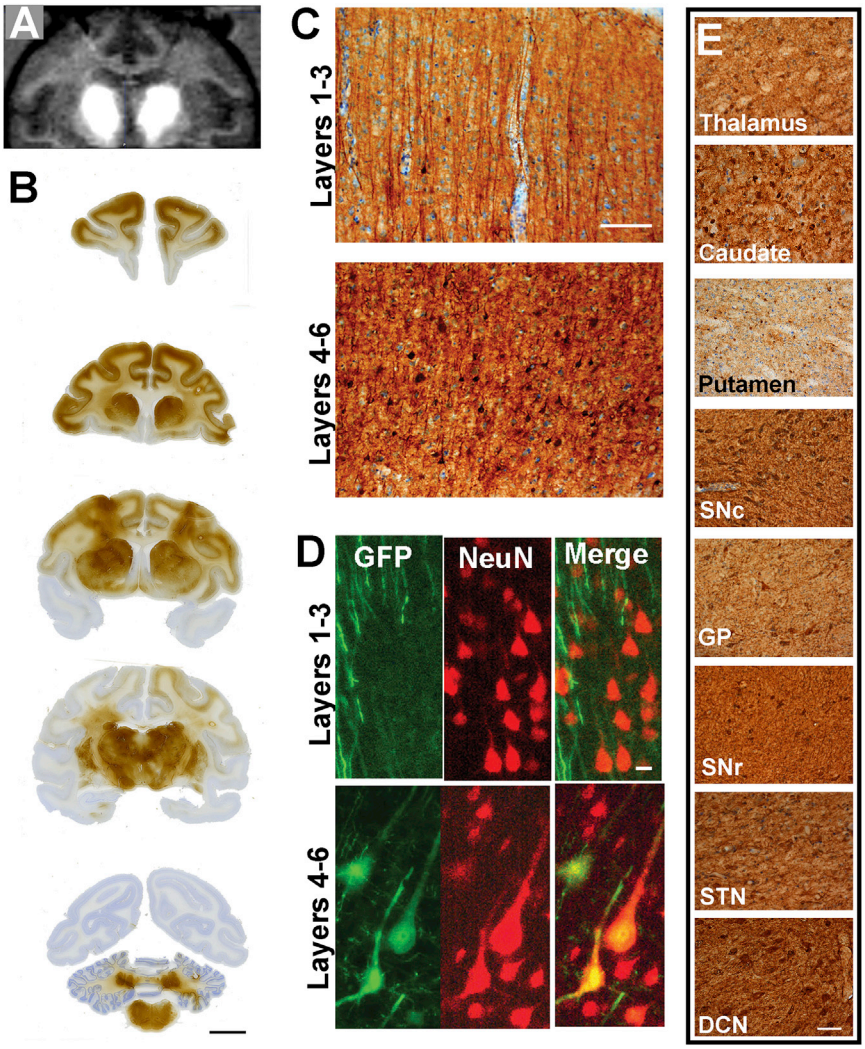

Figure 1. Histological Analysis of the Non-human Primate Brain after MRI-Guided Thalamic Infusion of AAV2-HBKO

(A) Bilateral delivery of AAV2-HBKO-GFP under intraoperative MRI guidance. MRI in the coronal planes showed that gadolinium signal was mostly contained within the thalamus. (B) Low-magnification images showing GFP staining in the prefrontal, frontal, and parietal and temporal cortices, but no GFP expression in the occipital cortex. GFP expression was also evident in several subcortical regions. Scale bar: 1 cm. (C) High-magnification images of 3,3'-diaminobenzidine (DAB) immunohistochemical staining showing primarily fiber transduction in layers 1–3 and cellular transduction in layers 4–6. Scale bar: 50 μm. (D) Double-immunofluorescent staining demonstrated colocalization of GFP and the neuronal nuclei marker NeuN in layers 4–6. Scale bar: 50 μm. (E) Panel of high-magnification images of DAB staining showing GFP expression in the thalamus, caudate, putamen, substantia nigra pars compacta (SNc), globus pallidus (GP), substantia nigra pars reticulata (SNr), subthalamic nucleus (STN), and deep cerebellar nuclei (DCN). Scale bar: 100 μm.

thalamus or cortex, and none of the animals presented any gross adverse clinical signs throughout the duration of the study. ICV infusion of AAV2-HBKO evinced transduction throughout the cerebral cortex (Figure 4B). Quantification of the area of GFP transduction relative to the total cortical area revealed that 65% of the prefrontal and frontal cortex, 60% of the temporal and parietal cortex, and 37% of the occipital cortex were transduced. Strikingly, ICV injections resulted in a cortical transduction pattern that was non-uniform and formed rosettes of oligodendrocytes interspersed with some neurons. The rosettes often surrounded blood vessels. Expression of GFP was mostly localized to superficial cortical layers (layers 1–3), although some patches of expression were observed in deeper layers (Figure 4C). Double-immunofluorescent double-labeling experiments were performed to quantify the phenotype of transduced cells, in which GFP expression was coupled with Olig2, a marker for oligodendrocytes, NeuN, a marker of neurons, or GFAP, a marker of astrocytes (Figure 4D). Of the total population of transduced cells, neurons accounted for 8%–18% of transduced cells in the shallow cortical layers and 13%–29% in the deep cortical layers (Figures 2A and 2B). Oligodendrocytes accounted for 75%–77% of transduced cells in shallow cortical layers and 74%–82% in deep cortical layers (Figures 2C and 2D).

ICV infusion did not result in any subcortical expression, but high levels of ependymal cell transduction lined the lateral ventricle (Figure S2). GFP-positive cells were present in all levels of the spinal cord (i.e., cervical, thoracic, lumbar, and sacral; Figure 3A) in both the dorsal and ventral horns. Quantification of the number of transduced motor neurons revealed that ICV delivery alone resulted in transduction of 93% of motor neurons at the cervical region, 84% in the thoracic, 85% in the lumbar, and 93% in the sacral regions (Figures 3A–3C).

Combination of ICV and Thalamic AAV2-HBKO Infusion Results in Widespread Oligodendrocyte Transduction in Superficial Cortical Layers, Neuronal Transduction in Deep Cortical Layers, and Robust Motor Neuron Transduction in the Spinal Cord

NHPs in this group received a combined bilateral ICV infusion and unilateral thalamic infusion (n = 2) under MRI guidance (1.8×10^{13} vg in ICV hemisphere and 2.0×10^{13} vg in combined ICV plus thalamic hemisphere). As with the other groups, no adverse events were observed during the infusion in the vasculature or parenchyma. AAV2-HBKO was rapidly distributed through the ventricular system and central canal within 5 min of starting the infusion. A small amount of vector leakage occurred into the STN in the hemisphere that received thalamic infusion, but no infusate was observed in

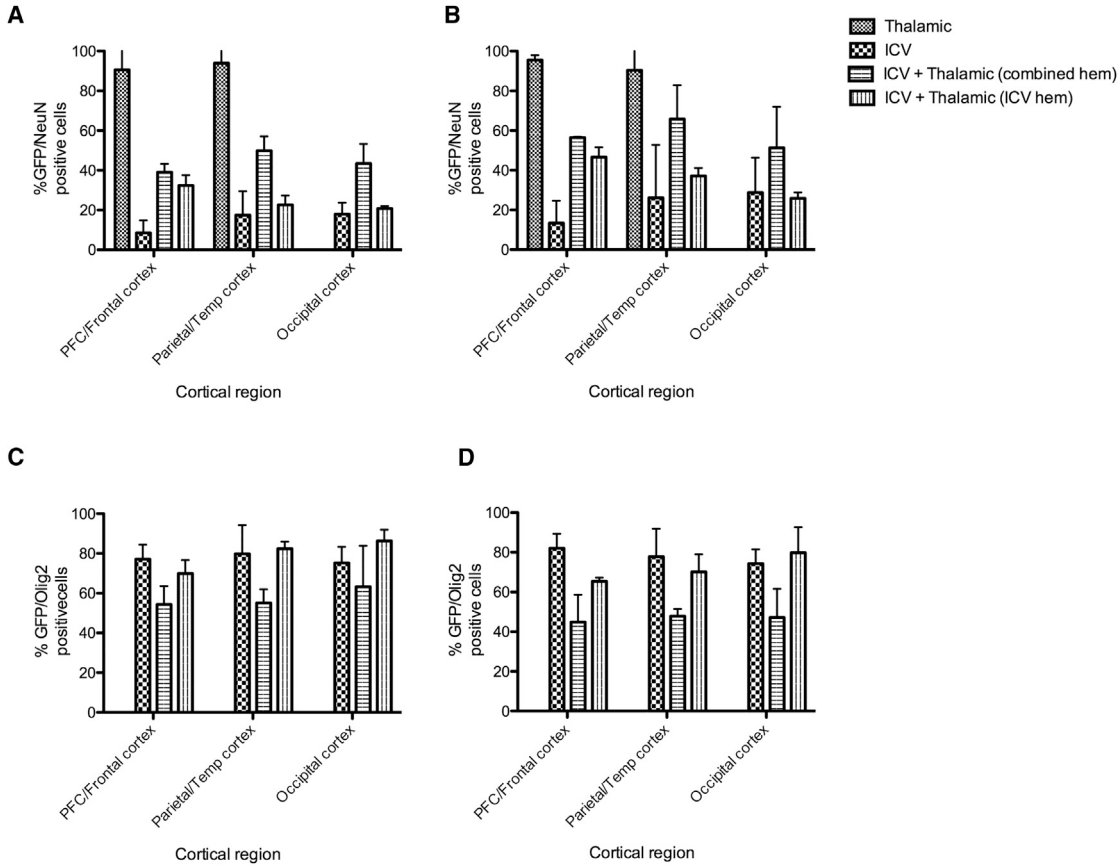

Figure 2. Percentage of Transduction in Each Cortical Region after Different Routes of AAV2-HBKO Delivery

Bar graphs showing that the percentage of GFP-transduced cells that colocalized NeuN was larger after thalamic infusion alone and with combined ICV and thalamic delivery, compared with ICV delivery alone in cortical layers 1–3 (A) and 4–6 (B). By contrast, the percentage of GFP-transduced cells that colocalized with Olig2 was large with ICV delivery and combination of ICV and thalamic, and largely confined to layers 1–3 (C) with minimal transduction of oligodendrocytes observed in layers 4–6 (D). Error bars are expressed as SEM.

neighboring non-target areas (Figure 5A). H&E staining revealed the presence of some perivascular cuffing and cellular infiltration at the injection site in the thalamus in the hemisphere that received the combination of ICV and thalamic delivery, along with an increase in GFAP and Iba1 immunoreactivity indicative of a clear immune response. H&E, GFAP, and Iba1 immunostaining revealed evidence of a mild immune response in the cortex in the hemisphere that received ICV delivery alone (Figure S3). There was no evidence of neuronal loss from visual examination of NeuN staining, and none of the animals presented any gross adverse clinical signs throughout the study.

Cortical transduction was observed in both hemispheres (Figure 5B). In the hemisphere that received combined ICV and thalamic delivery, transduction was observed in 94% of the total prefrontal and frontal cortical area, in 39% of the temporal and parietal cortical area, and in 20% of the occipital cortical area. The hemisphere that received only the ICV injection displayed transduction in 66% of the prefrontal and frontal cortical area, in 56% of the parietal and temporal cortex, and 63% of the occipital cortex. The combination of ICV and thalamic delivery resulted in transduction of primarily oligodendrocytes in superficial layers and neuronal transduction in deeper layers (Figures 5C and 5D). Phenotypic quantification of GFP-transduced cells showed that oligodendrocytes accounted for 54%–63% of the total population of transduced cells in the superficial layers and 45%–48% of transduced cells in deep cortical layers (Figures 2C and 2D). Neuronal transduction was evident in 39%–50% of transduced cells in superficial cortical layers and 51%–66% of transduced cells in deeper cortical layers (Figures 2A and 2B). Interestingly, a lower percentage of neuronal transduction was evident in the hemisphere that received ICV infusion alone (21%–32% of transduced cells in superficial cortical layers and 26%–47% in deep cortical layers) compared with the hemisphere that received both the thalamic and the ICV infusion (Figures 2A and 2B). AAV2-HBKO infusion did not result in astrocytic transduction in any treatment group (data not shown).

Similar to the ICV group, the hemisphere that received combined thalamic and ICV infusion displayed bidirectional axonal transport

Table 1. Summary of Axonal Transport 4 Weeks after Infusion of AAV2-HBKO into the Non-human Primate Thalamus

Structure	Anterograde Transport	Retrograde Transport
Cerebral cortex	√	–
Caudate + putamen	–	√
Globus pallidus	–	√
SNr	–	√
SNc	–	√ (secondary transport[a])

SNc, substantia nigra pars compacta; SNr, substantia nigra pars reticulata.
[a]GFP expression in the SNc occurred via secondary anterograde axonal transport from a primary transduction zone in either the subthalamic nucleus or putamen.

to several subcortical regions. GFP staining was evident in the caudate and putamen, globus pallidus, SNr, and SNc (Figure 5E). High levels of GFP transduction were observed in ependymal cells bilaterally (Figure S2). Quantification of motor neuron transduction revealed 94% transduction at the cervical level, 98% at the thoracic level, 90% transduction at the lumbar level, and 76% in the sacral region (Figure 3C). There were no differences between the left and right spinal cord (data not shown).

DISCUSSION

AAV2 vectors bind HSPGs on the cell surface of neurons and, unlike other vector capsid-receptor interactions, its affinity for HSPGs impedes the spread of the vector beyond the injection site somewhat.[10] AAV serotypes that do not bind to HSPGs (such as AAV1, AAV5, and AAV9) tend to show increased distribution after direct injection into the brain, implicating heparan binding as a barrier to widespread CNS transduction.[12,14,15] Distributing transgenes widely throughout the brain has obvious implications for the treatment of many neurological disorders. In order to establish the potential clinical utility of a non-heparan binding AAV2 vector, we evaluated a novel AAV2-HBKO capsid in a large mammalian brain with the ultimate goal of targeting widespread regions of the human brain with AAV vectors to direct therapeutic transgene expression.

The most notable finding of the present study was the discovery that ICV delivery of AAV2-HBKO resulted in an entirely different cell transduction pattern compared with thalamic delivery. ICV delivery of AAV2-HBKO resulted in transduction of oligodendrocytes in the cortex and motor neuron transduction in the spinal cord. In contrast, thalamic infusion resulted in entirely neuronal transduction in both the brain and spinal cord; no oligodendrocyte transduction was observed in any regions evaluated.

Oligodendrocytes may be preferentially transduced by ICV delivery as a result of vector flow into the perivascular space, which is in direct contact with oligodendrocytes, leaving a smaller proportion of vector particles available to transduce neurons. This idea is consistent with the rosette pattern of transduction we observed surrounding blood vessels. To our knowledge, AAV2 has yet to be assessed by cerebrospinal fluid (CSF) delivery in the NHP, but we observed a similar rosette pattern of transduction with cisterna magna delivery of both AAV7 and AAV9.[29] Astrocytes, which are also in direct contact with CSF, were the primary cell type transduced by AAV7 and AAV9. AAV9 does not bind to HSPGs, indicating that removal of the HSPG receptor binding capability is not in itself sufficient to shift cellular tropism of AAV vectors toward oligodendrocyte transduction. Removal of the HSPG receptor binding site may release steric hindrance allowing other receptor binding sites present on AAV2 vector (that are not present on AAV9) to bind to oligodendrocytes. A direct comparison of AAV2 and AAV2-HBKO by CSF delivery is warranted in order to define clearly the role of HSPG binding on oligodendrocyte transduction. Consistent with what we have described for AAV2,[16] AAV2-HBKO vector maintained the neuronal tropism of the parental AAV2 capsid after thalamic delivery, a characteristic that makes AAV2-HBKO an attractive vector for the treatment of neurodegenerative diseases. Route of delivery has been shown to impact tropism of AAV vectors previously,[30,31] but to our knowledge this is the first time cortical oligodendrocyte transduction has been reported.

The robust spinal cord transduction observed with ICV delivery has important implications for diseases that primarily impact lower motor neuron function. Our finding that AAV2-HBKO transduced primarily oligodendrocytes in the brain, but only motor neurons in the spinal cord, may be explained by the fact that a different subtype of oligodendrocytes is present in the gray matter of the brain, i.e., non-myelinating satellite oligodendrocytes, versus myelinating oligodendrocytes in the spinal cord.[32] Satellite oligodendrocytes in the gray matter of the brain express a different repertoire of cell surface receptors that set them apart from the myelinating oligodendrocytes found in the spinal cord.[32] It is possible that the HSPG receptor binding site sterically hinders binding and internalization of AAV2 vector with other receptors. Abolition of the HSPG binding capabilities may thus allow for binding and internalization by receptors found on satellite oligodendrocytes that are not present on myelinating oligodendrocytes. Basic fibroblast growth factor (bFGF) receptor has been identified as a co-receptor for successful entry of AAV2 vector into host cells,[33] so it is possible that the bFGF receptor was utilized by AAV2-HBKO for entry into either oligodendrocytes or neurons in the present study. Indeed we have previously found that bFGF can act as an adjuvant to enhance distribution of AAV2 in the rat brain,[19] but this hypothesis requires further investigation.

The widespread transduction of cortical oligodendrocytes in the present study is unprecedented for several reasons. First, most widely explored AAV serotypes exhibit a predominantly neuronal tropism. Some AAV serotypes possess a weak tropism for oligodendrocytes when the myelin basic promoter is used, but the overall transduction of oligodendrocytes reported is still low.[34,35] Second, in studies that have reported tropism for oligodendrocytes, transduction has been limited to subcortical areas, and only at the site of parenchymal infusion. For example, we have found that infusion of AAV1 into the corona radiata of NHPs leads to transduction of oligodendrocytes in white matter at the infusion site, but not in any other regions of

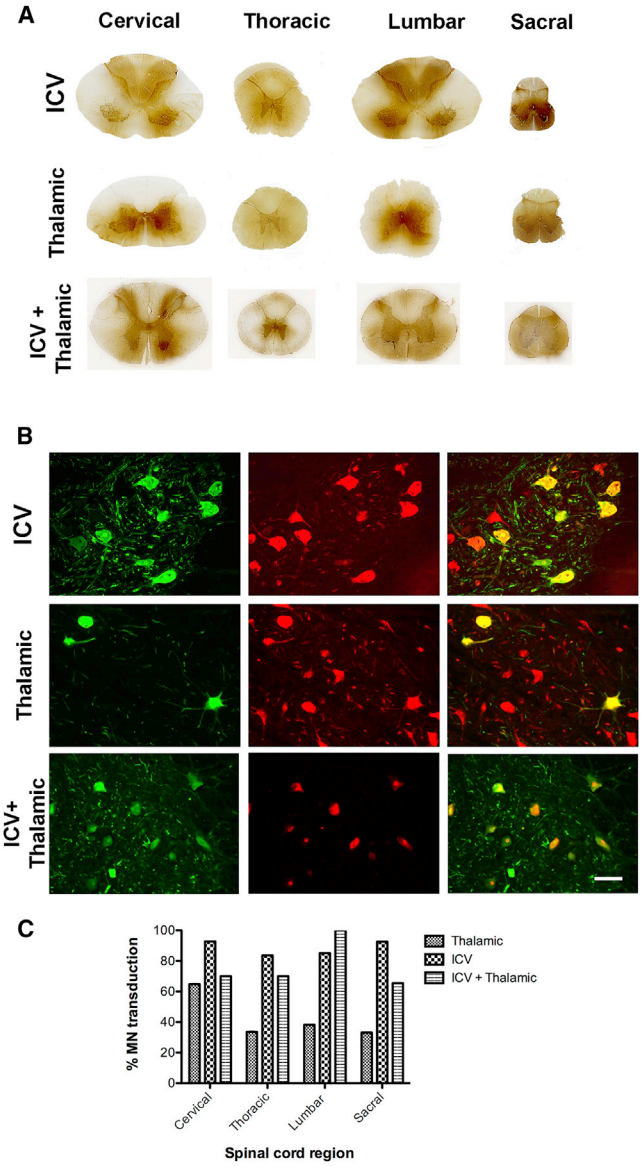

Figure 3. Robust Motor Neuron Transduction in the Spinal Cord after Different Routes of AAV2-HBKO-GFP Delivery

(A) GFP-positive cells were found at cervical, thoracic, lumbar, and sacral spinal regions after chromogenic immunostaining in ICV, thalamic, and combined ICV and thalamic groups. Scale bar: 1 cm. (B) Double-immunofluorescent staining showed GFP and large NeuN-positive motor neurons that colocalized with GFP (merge). Scale bar: 50 μm. (C) Graph showing quantification of motor neuron transduction as a percentage of total motor neurons.

the brain.[30] Similarly, McCown and colleagues[36] described an AAV variant that demonstrated high oligodendrocyte transduction levels in the corpus callosum and striatum but did not report any transduction outside of the infusion site.

Indeed the present study indicates that both vector capsid and route of delivery are key factors in determining tissue distribution and tropism in the brain. To our knowledge, this is the first time ICV delivery of AAV vector has been described in NHP. The total dose administered was higher than with the thalamic infusions to account for dilution of vector particles within the CSF. Intra-operative MRI demonstrates that ICV delivery of AAV vectors is an inherently efficient process that rapidly distributes AAV vector throughout the brain and spinal cord (a total infusion time of 1.5 min). In addition to the pace of CSF flow and compliance of this compartment for large volumes of vector, ICV injection has the added advantage of following the inherent direction of CSF flow. On that basis, one might predict that ICV delivery of AAV vector would be a more efficient distribution modality than the cisterna magna and lumbar injections more commonly used for CSF delivery.

The present study also highlights important distinctions between the axonal transport properties of AAV2-HBKO and AAV2. In our experience, the axonal transport profiles of a particular vector can be impacted by: (1) the neuroanatomical site of infusion, (2) capsid modification, (3) vector purification method, and (4) vector titer. With the exception of one study that is discussed in detail below,[21] AAV2, in our hands and in the hands of other groups, typically undergoes primarily anterograde axonal transport in NHP.[1,16,24]

The thalamus projects primarily to the cerebral cortex, but also sends afferent projections to the striatum, and receives efferent projections from the globus pallidus (internal), the SNr, and the cerebellum. Thalamic infusion of AAV2-HBKO resulted in robust anterograde transport to the cortex, and both anterograde and retrograde axonal transport to transduce several subcortical regions in addition to the site of injection in the thalamus. Anterograde axonal transport of AAV2-HBKO was evident from GFP staining in the striatum via thalamostriatal projections. Robust retrograde transport was discernible from transduction of the globus pallidus, SNr deep cerebellar nuclei, and brainstem. This finding is distinct from what we have previously found with thalamic injection of AAV2 in the primate brain at a comparable titer.[16] In that study we found that AAV2 transduced only the injection site in the thalamus and the cortex, but no other subcortical regions were transduced (Figure S5). This finding suggests that AAV2-HBKO may have a higher propensity for both anterograde and retrograde axonal transport compared with AAV2. In the present study, cortical transduction extended from the prefrontal cortex to areas of parietal and temporal cortex just above the brainstem. The lack of occipital cortex transduction is likely due to inefficient primary transduction of the lateral geniculate nucleus, which projects to the primary visual cortex. The robust brainstem transduction observed after thalamic delivery of AAV2-HBKO is unprecedented, as this area is very difficult to target for gene delivery. All untransduced regions of the brain do not have any direct afferent or efferent connections from the site of injection in the thalamus.

The spinal cord transduction with thalamic delivery indicates that AAV2-HBKO may undergo transsynaptic transport, because there is no direct pathway from the thalamus to the spinal cord. Thalamic

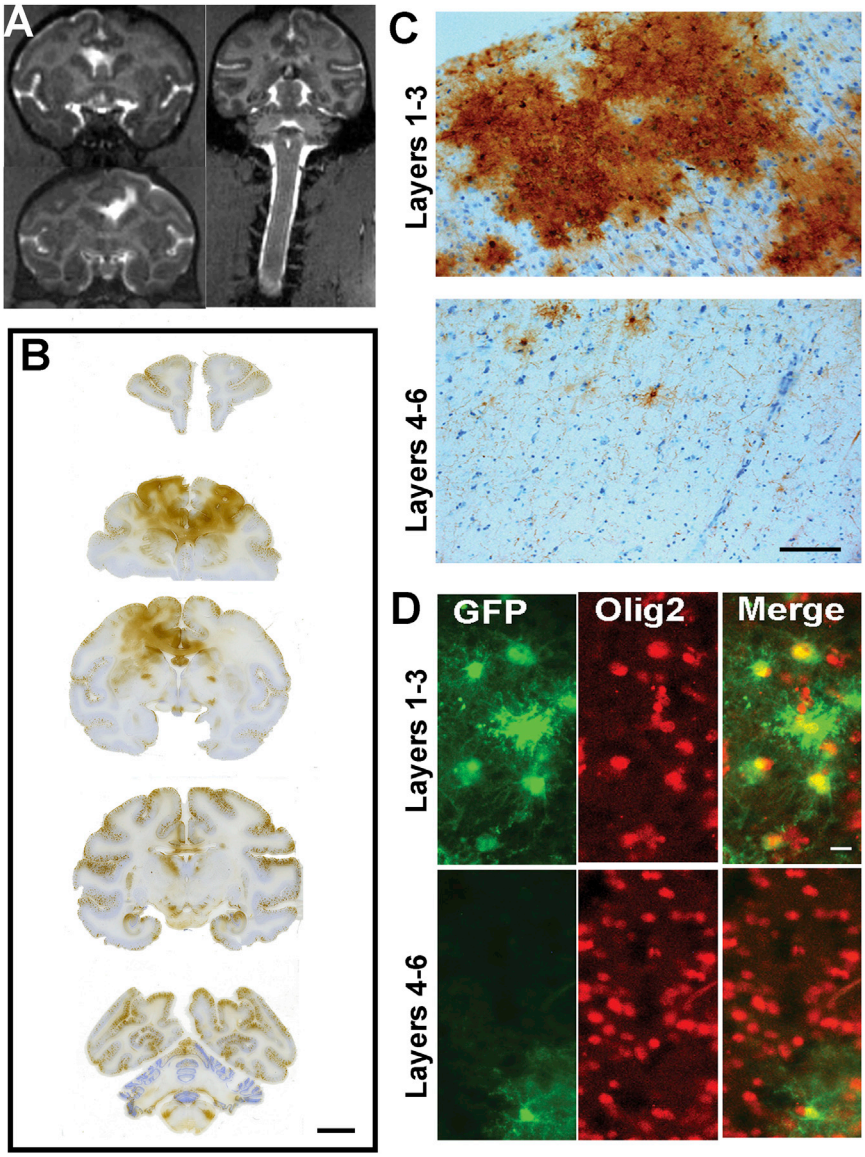

Figure 4. Histological Analysis of the Non-human Primate Brain after MRI-Guided Intracerebroventricular Infusion of AAV2-HBKO

(A) MR image in coronal plane showing gadolinium signal in the CSF at the end of the 1.5-min infusions. Gadolinium signal was mostly contained within the lateral ventricles and was observed following the flow of CSF through the ventricular system and central canal. (B) Low-magnification brain images showing GFP staining throughout the brain in the prefrontal, frontal, parietal and temporal cortex, and occipital cortices. No GFP expression was evident in subcortical regions. Scale bar: 1 cm. (C) High-magnification images of DAB immunohistochemical staining showing robust GFP expression in rosettes in cortical layers 1–3 and very sparse GFP staining in cortical layers 4–6. Scale bar: 50 μm. (D) Double-immunofluorescent staining revealed colocalization of GFP and the oligodendrocyte marker Olig2 in cortical layers 1–3 and 4–6. Scale bar: 50 μm.

infusion of AAV2-HBKO resulted in anterograde axonal transport along the thalamocortical tract to transduce pyramidal cells in layer V of the cortex, then by anterograde transport along the corticospinal tract to transduce interneurons and motor neurons in the ventral horn of the spinal cord. AAV2-HBKO also underwent retrograde axonal transport via the spinothalamic tract to transduce the dorsal spinal cord. This could have occurred either directly along second-order neurons projecting directly from the thalamus to the ventral horn of the spinal cord, or transsynaptically, first via anterograde transport along first-order neurons to the somatosensory cortex, followed by retrograde transport along second-order neurons to the ventral spinal cord. Transsynaptic transport occurred exclusively from the cortex, not all secondary transduction sites. Further studies are required to examine vector particle distribution in secondary and tertiary transduction regions to determine whether this phenomenon is a function of vector particle concentration. Thalamic infusion of AAV2-HBKO could potentially be useful for devastating motor neuron diseases, such as amyotrophic lateral sclerosis (ALS), which affects both upper and lower motor neurons.

Axonal transport properties may also be affected by the vector purification method. As mentioned, to our knowledge, we are the only group to have reported that AAV2 can undergo both anterograde and retrograde transport in the NHP brain,[20] when purified with a column chromatography method different from the more commonly used stringent cesium chloride purification method.[1,24] The present study is similar to the AAV2 described in Hadaczek et al.[21] in the sense that both of the vectors were produced with the same proprietary purification method, were injected at comparable titers, and both preparations had comparable purity, ratio of empty to full, and presence of contaminants. Both studies investigated distribution of the respective vectors after parenchymal delivery, but AAV2 was administered into the putamen by Hadaczek et al.,[21] whereas AAV2-HBKO was delivered into the thalamus in the present study. Bidirectional axonal transport was observed in both studies, but infusion of AAV2 into the putamen resulted in incomplete transduction in some subcortical regions (e.g., the thalamus). AAV2-HBKO, by contrast, resulted in complete transduction of all of the same subcortical regions as with AAV2 in Hadaczek et al.[21] A direct comparison of AAV2 and AAV2-HKO purified by the same method and infused into the same target site in the primate brain would be of interest in future studies in order to further elucidate the full contribution of HSPG binding to vector transport.

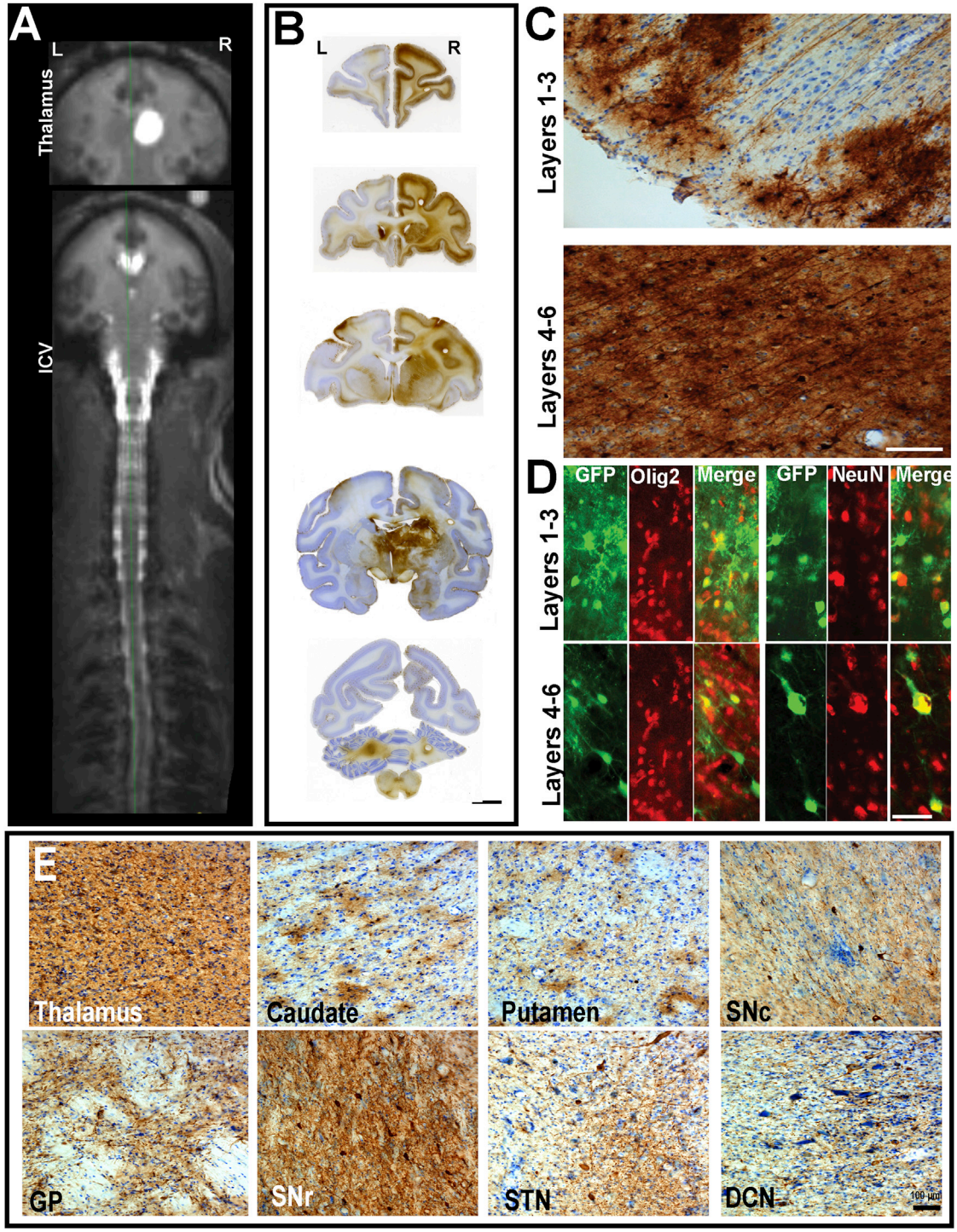

Figure 5. Histological Analysis of the Non-human Primate Brain after MRI-Guided Combined Thalamic and Intracerebroventricular Infusion of AAV2-HBKO

(A) MR images in the coronal plane showing gadolinium signal at the end of the ICV and thalamic infusions. Gadolinium signal was mostly contained within the thalamus in the right hemisphere (top) and with the lateral ventricle. The infusate was observed following the flow of CSF through the ventricular system and central canal (bottom). (B) Low-magnification brain images showing GFP immunostaining. In the ICV hemisphere (left), GFP expression was evident in the prefrontal, frontal, parietal and temporal cortex, and occipital cortices. No GFP expression was evident in subcortical regions. In the ICV and thalamic combination hemisphere (right), GFP expression was evident in the prefrontal, frontal, parietal and temporal cortex, and occipital cortices along with several subcortical regions. Scale bar: 1 cm. (C) High-magnification images of DAB

(legend continued on next page)

Vector dose may also be an important factor influencing axonal transport directionality. In the present study, we injected 1.6–3.4 × 10^{12} vg of AAV2-HBKO per thalamus. We have previously shown strong dose dependency of axonal transport with other serotypes. Notably, retrograde axonal transport triggered with AAV9, at 1.5 × 10^{12} vg,[37] and with AAV5 in the range of 1.0–1.5 × 10^{12} vg.[38] We would argue, therefore, that retrograde transport of AAV2-HBKO may be decreased at lower titers, a hypothesis that requires further investigation.

The results presented here also highlight the important message that rodent data do not always translate to the primate brain. We cannot presume that a route of delivery that produces a particular pattern of distribution and tropism in rodents and other small mammals will reproduce in the NHP or humans. Manfredsson and colleagues[22] have evaluated the impact of AAV2 HSPG binding on transduction in the rat brain, but they have not described axonal transport after intraparenchymal infusion of an analogous AAV2 deficient in HSPG binding into the striatum. AAV2-HBKO, by contrast, underwent robust axonal transport in both NHP and mice.[20] The AAV2 capsid variant described by Manfredsson and colleagues[22] (referred to as T2 3Y +T +dH) had several mutations to the canonical HSPG-binding residues. The AAV2-HBKO-based vector used in our study substituted two positively charged arginine residues (R585A and R588A) for two hydrophobic alanine residues on the surface of the AAV2 capsid, thereby ablating the AAV2 capsid-HSPG interactions. The effect of abrogating HSPG binding was solely evaluated in this study. It is possible that R585A and R588A play important roles in the axonal transport properties of AAV2 vector, and that the substitution with hydrophobic alanine residues resulted in the bidirectional axonal transport observed in the present study. Due to the number of mutations contained in the Manfredsson variant, the contributions of any individual mutation and the contribution of species-specific differences in transduction profiles cannot be fully disentangled.

In rodents, ICV delivery of AAV2 restricts transduction to ependymal cells and offers very little expression outside of the ependymal.[39–41] Both robust ependymal cell transduction and widespread cortical transduction were observed in the present study, indicating that abolition of HSPG binding capability increases the propensity to overcome complete sequestration of all vector particles to ependymal cells, enabling for delivery of remaining vector particles to the cortex. Vector titer differences could also explain some dissimilarities in distribution between rodents injected with parent AAV2, the variant described by Manfredsson and colleagues,[22] and the AAV2-HBKO described in the present study. NHPs were infused with AAV2-HBKO at a titer of 1.2 × 10^{13} vg/mL, whereas Manfredsson and colleagues[22] injected rats with their HSPG binding variant at a lower titer of 1.2 × 10^{12} vg/mL, and parent AAV2 vector was injected at titers as low as 1 × 10^{9} vg/mL.[39–41] Dose-ranging experiments in both rodents and NHPs would enable the effect of titer to be extricated from HSPG binding capability.

The volume of vector relative to CSF volume is another important factor to consider. In the present study, a total of 3 mL of vector was injected, representing approximately 20% of the normal volume of CSF in a normal NHP (~12–15 mL). The volume typically infused into rats is comparatively lower, and typically a 10-μL infusion is administered representing less than 5% of the normal volume of CSF in a rat (~250–350 μL). Due to these differences, in addition to the low number of NHP used in the present study, it is difficult to draw final conclusions about the relationship between dose, volume, and transduction. It is possible that there is a threshold of vector particles in a given volume of CSF that is required to overcome sequestration to ependymal cells, leading to transduction in the cortex. The comparatively lower concentration of vector particles in CSF in the rodent studies may not have exceeded the required number of vector particles to maximally quench ependymal cell transduction and lead to cortical transduction. Another hypothesis to explain this phenomenon is differential binding affinities across species, which might sequester vector to the different cell types more readily in some species.

The concept of paradoxical AAV transduction profiles in rodents versus higher mammals was exemplified recently by Wilson and colleagues,[23] who showed that the AAV9 variant AAV-PHP.B that demonstrated remarkable global transduction of the CNS after intravenous delivery in mice[42] was functional only in the model in which it was selected, i.e., a Cre transgenic mouse in a C57BL/6J background, but resulted in only very low CNS transduction in NHPs and another commonly used mouse strain BALB/cJ. These data serve as a cautionary tale highlighting the importance of assessing biodistribution of viral vectors in large mammals prior to clinical use.

AAV2-HBKO was well tolerated by all subjects regardless of the route of delivery with no gross adverse clinical signs throughout the study. Congruent with previous studies, the high level of GFP expression in primary transduction zones caused some perivascular cuffing, astrocytic activation, and microglial hyperactivity at primary injection sites. We found evidence of mild toxicity in secondary sites, implying that the local inflammatory response was likely due to sequestration of GFP-containing vector particles in the infusion site. Although GFP is valuable when used as a cellular tag to measure gene expression and cell tracking, there is a wealth of evidence to suggest high levels of GFP can produce immunogenicity and toxicity when expressed in antigen-presenting cells over a period of time, i.e., >4 weeks.[26,43] Clinical vectors would not contain the GFP

immunohistochemical staining in the cortex showing robust GFP expression in rosettes in layers 1–3 and nuclei and fiber staining in layers 4–6. Scale bar: 50 μm. (D) Panel shows high-magnification images of double-immunofluorescent staining in the combined ICV and thalamic hemisphere. GFP-positive cells colocalized with Olig2 in layers 1–3. A small proportion of GFP-positive cells colocalized with NeuN in layers 1–3. In layers 4–6, the majority of GFP-positive cells colocalized with NeuN, and a small proportion of GFP-positive cells colocalized with Olig2. Scale bar: 50 μm. (E) DAB staining in the ICV and thalamic hemisphere showing GFP expression in the thalamus, caudate, putamen, substantia nigra pars compacta (SNc), globus pallidus, SNr, subthalamic nucleus (STN), and deep cerebellar nuclei (DCN). Scale bar: 100 μm.

transgene and are thus unlikely to cause the immunogenicity seen at the primary injection sites.

In summary, these findings demonstrate that binding of AAV2 to HSPGs significantly impacts AAV2-mediated transduction in the NHP CNS, and the route of delivery significantly impacts both vector distribution and tropism. We have shown that AAV2-HBKO undergoes extensive bidirectional axonal transport and therefore has considerable potential for the delivery of therapeutic candidate genes, where more global transduction of the brain is required. Further experiments will be needed to obtain a more comprehensive understanding of the axonal transport abilities observed with this vector. Our data demonstrate a valuable example of how modification of capsid-receptor interactions can change transduction profiles of AAV vectors and can be used to tailor AAV gene therapy vectors for clinical application. These findings also underscore the importance of identifying the appropriate vector serotype in conjunction with the optimal route of delivery to selectively deliver transgenes of interest to the CNS for the treatment of neurological disorders.

MATERIALS AND METHODS

Generation of AAV Capsid Mutant Plasmids

Mutagenesis was performed with the QuikChange Lightning Multi Site-Directed Mutagenesis kit following the manufacturer's protocol (Agilent Technologies, Santa Clara, CA, USA). The single-stranded AAV2-HBKO plasmid was generated by a PCR mutagenesis primer designed to introduce two mutations of arginines 585 and 588 to alanines into the parent rep/cap plasmid pIM45BD, a substitution that is repeated 60 times over the capsid surface. These mutations have previously been shown to abolish the HSPG receptor binding capability of AAV2.[44] The sequence of the mutagenesis primer used to introduce the R585A and R588A mutations was 5′-TATCTAC CAACCTCCAGGCAGGCAACGCACAAGCAGCTACCGCAG-3′, and the presence of the mutations was confirmed by sequencing.

AAV Vector Production

AAV vectors carrying the EGFP gene under the control of the chicken β-actin (CBA) promoter were produced by a transient transfection production method as previously described.[45] In brief, HEK293 cells were transfected with polyethyleneimine (PEI) and a 1:1:1 ratio of the three plasmids (ITR vector, AAV rep/cap, and Ad helper plasmid). The Ad helper plasmid used, pHelper, was obtained from (Stratagene/Agilent Technologies, Santa Clara, CA, USA). Purification of the vector was performed by column chromatography as previously described.[46] The vector preparation was substantially free of contaminants, as assessed by SDS-PAGE analysis with SYPRO staining; additionally the fractional content of empty capsids in the vector preparation was low at 13%, as determined by analytical ultracentrifugation (Figure S4).[47]

Non-human Primates

Eight adult male Rhesus macaques (*Macaca mulatta*) were screened for neutralizing antibodies against AAV2 prior to surgery as previously described.[11,24,37] Animals considered seronegative (serum titers < 1:25) were included in the study. Each animal received AAV2-HBKO-CBA-EGFP at a concentration of 1.2×10^{13} vg/ mL bilaterally into either the thalamus (n = 3; 130–280 μL per hemisphere), ICV (n = 3; 1.5 mL per hemisphere), or both ICV and thalamus (n = 2; 1.5 mL per ventricle and 200 μL per thalamus) under MRI-guided CED[48–50] with an adjustable stepped catheter (MRI Interventions, Irvine, CA, USA). The vector was mixed with a gadolinium-based magnetic resonance (MR) contrast agent diluted to 2 mM (ProHance H; Bracco Diagnostics, Princeton, NJ, USA) to enable visualization of the infusion in real time. The animal's head was placed in a MRI-compatible stereotactic frame, and a craniotomy was performed. The NHP was then moved to a 1.5T MRI GE scanner where T1-baseline images were acquired. Trajectory of the cannula relative to the target structures was determined with OsiriX software (Geneva, Switzerland). For the thalamic infusions the vector was infused at 1 μL/min while the cannula was inserted, then at 3–5 μL/min for the remainder of the infusion. ICV infusions involved infusion of vector at 1 μL/min and an increase in the flow rate to 10 μL/min once gadolinium signal was visualized in the target area. A transfrontal trajectory was utilized for both thalamic and ICV infusions.[51]

Tissue Processing

Animals were injected with a lethal dose of sodium pentobarbital 21 days after surgery, followed by transcardial perfusion with 0.1 M PBS and then fixation with 4% paraformaldehyde/PBS. The brains were removed, sliced into 6-mm coronal blocks, and along with the spinal cords, were post-fixed by immersion in 4% paraformaldehyde/PBS overnight. The next day, the brain and spinal cord were transferred to 30% (w/v) sucrose. GFP expression analysis was determined in 40-μm brain sections with a monoclonal antibody against GFP (rabbit anti-GFP, 1:1,000; G10362; Thermo Fisher Scientific, San Francisco, CA, USA). Motor neuron transduction was determined in 15-μm spinal cord sections immunostained with monoclonal antibodies against GFP and NeuN (mouse anti-NeuN, 1:5,000; mab377; Millipore, Temecula, CA, USA) on consecutive sections. A cresyl violet counterstain was performed on all sections to identify brain and spinal cord structures relative to transduced areas as previously described.[28,38,52] Standard H&E staining was performed in all animals in order to assess possible pathological signs. Astrogliosis and microglial hyperactivity were assessed by staining with antibodies directed against a marker of astrocytes (mouse monoclonal anti-GFAP, 1:15,000; mab360; Millipore, Temecula, CA, USA) and a microglial marker (rabbit polyclonal anti-Iba1, 1:1,000; CP290C; Biocare Medical, Pacheco, CA, USA) as previously described.[29,43,52]

Double-Immunofluorescent Staining

The phenotype of GFP-positive cells was examined by double-immunofluorescence staining. Brain sections were washed with 0.1 M PBS + Triton (PBST), blocked for 1 hr in 20% normal horse serum (Jackson ImmunoResearch), and then incubated overnight at 4°C with a mixture of anti-GFP and a specific antibody for oligodendrocytes (anti-Olig 2, mouse monoclonal, 1:100, MAB377; Millipore). After

incubation with primary antibodies, sections were washed in PBST, incubated with a cocktail of the corresponding secondary antibodies in PBS for 2 hr at room temperature, washed in PBS, and mounted on frosted slides. To avoid autofluorescence due to lipofuscin, sections were incubated in 0.3% Sudan Black B solution for 5 min and then washed in PBS followed by distilled water.

Motor Neuron Cell Counting

The number of transduced motor neurons in the spinal cord was determined on sections doubly immunostained with anti-GFP and anti-NeuN antibodies. The number of GFP-positive cells was compared with the total number of motor neurons. Cell transduction was quantified by manual cell counting bilaterally along the rostrocaudal axis of the cervical, thoracic, lumbar, and sacral segments. Large cell bodies located in laminae 8 and 9 (ventral horn) of the spinal cord were considered motor neurons. Approximately 4–6 sections were selected for each spinal cord segment to generate the overall mean number of motor neuron counts transduced per segment for each animal. Care was taken to anatomically match sections between animals.

Quantification of Cortical Transduction

Representative images were captured of representative whole-brain sections from the prefrontal, frontal, parietal, and occipital cortices that had undergone chromogenic anti-GFP staining at 1,200 dots per inch (dpi) with an Epson Perfection V700 Photo Scanner. The region of interest (ROI) tool in ImageJ was used to delineate the transduction area and total cortical area with the ROI manager as previously described.[3] The percentage of cortical transduction was calculated by dividing the area of transduction by the total cortical area. Image processing was undertaken by an observer blinded to treatment group. The average cortical transduction from three sections spaced 480 μm apart was used to determine the "% cortical area" transduced for each cortical region.

Quantification of Cellular Tropism in the Cortex

To determine the percentage of oligodendrocyte and neuronal transduction of the total GFP transduction in the cortex, we selected representative sections from the prefrontal, frontal, parietal, and occipital cortices that had undergone double-immunofluorescent staining against either Olig2 or NeuN and GFP. Images were taken with a Zeiss Axioscope microscope equipped with a Zeiss Mrc5 camera at 40× magnification. Images were captured in 16 randomly selected areas per section (8 images in superficial cortical layers 1–3 and 8 images in the deep cortical layers 4–6) first under blue excitation (to visualize GFP) and then by red excitation (to visualize Olig2 or NeuN). As described previously,[8] ImageJ was used to automatically count the total number of GFP-positive, GFP and NeuN double-labeled, and GFP/Olig2 double-labeled cells with the "Threshold" command used to separate background from the cells, which were then counted with the "Analyze Particles" command. The RGB image was converted to grayscale (8 bit), and the threshold set. The ImageJ analysis algorithm was applied to count the cells with a cutoff area of less than 100 pixels (noise).

Study Approval

All procedures were carried out with the approval of the Institutional Animal Care and Use Committee (IACUC permit: AN 117108) and in accordance with the Standard Operating Procedures protocol at University of California, San Francisco, San Francisco, CA, USA.

SUPPLEMENTAL INFORMATION

Supplemental Information includes five figures and can be found with this article online at https://doi.org/10.1016/j.ymthe.2018.07.008.

AUTHOR CONTRIBUTIONS

J.N. conducted experiments, generated and analyzed data, and wrote the paper; L.M.S. designed the experiment, and wrote and edited the paper; K.O. conducted experiments and analyzed data; S.T. processed tissue and generated data; L.S. conducted experiments and edited the paper; P.H. provided management and oversight; C.O. generated vectors and edited the paper; J.S. conducted experiments; W.S.S. edited the paper; J.R.B. conducted experiments; C.S. processed tissue and managed laboratory resources; Amin Mahmoodi processed tissue; Amir Mahmoodi processed tissue; J.F. reviewed and edited the paper; K.S.B. developed and designed methodology, provided supervision and leadership, and reviewed the paper; L.S.S. conceptualized ideas and edited the paper.

CONFLICTS OF INTEREST

L.M.S., C.O., J.S., and L.S.S. are employees of Sanofi.

ACKNOWLEDGMENTS

This work was supported by Sanofi.

REFERENCES

1. Hadaczek, P., Eberling, J.L., Pivirotto, P., Bringas, J., Forsayeth, J., and Bankiewicz, K.S. (2010). Eight years of clinical improvement in MPTP-lesioned primates after gene therapy with AAV2-hAADC. Mol. Ther. *18*, 1458–1461.

2. Sehara, Y., Fujimoto, K.-I., Ikeguchi, K., Katakai, Y., Ono, F., Takino, N., Ito, M., Ozawa, K., and Muramatsu, S.I. (2017). Persistent expression of dopamine-synthesizing enzymes 15 years after gene transfer in a primate model of Parkinson's disease. Hum. Gene Ther. Clin. Dev. *28*, 74–79.

3. Jensen, E.C. (2013). Quantitative analysis of histological staining and fluorescence using ImageJ. Anat. Rec. (Hoboken) *296*, 378–381.

4. Hocquemiller, M., Giersch, L., Audrain, M., Parker, S., and Cartier, N. (2016). Adeno-associated virus-based gene therapy for CNS diseases. Hum. Gene Ther. *27*, 478–496.

5. Bobo, R.H., Laske, D.W., Akbasak, A., Morrison, P.F., Dedrick, R.L., and Oldfield, E.H. (1994). Convection-enhanced delivery of macromolecules in the brain. Proc. Natl. Acad. Sci. USA *91*, 2076–2080.

6. Morrison, P.F., Laske, D.W., Bobo, H., Oldfield, E.H., and Dedrick, R.L. (1994). High-flow microinfusion: tissue penetration and pharmacodynamics. Am. J. Physiol. *266*, R292–R305.

7. Varenika, V., Kells, A.P., Valles, F., Hadaczek, P., Forsayeth, J., and Bankiewicz, K.S. (2009). Controlled dissemination of AAV vectors in the primate brain. Prog. Brain Res. *175*, 163–172.

8. Grishagin, I.V. (2015). Automatic cell counting with ImageJ. Anal. Biochem. *473*, 63–65.

9. Kotterman, M.A., and Schaffer, D.V. (2014). Engineering adeno-associated viruses for clinical gene therapy. Nat. Rev. Genet. *15*, 445–451.

10. Mastakov, M.Y., Baer, K., Kotin, R.M., and During, M.J. (2002). Recombinant adeno-associated virus serotypes 2- and 5-mediated gene transfer in the mammalian brain: quantitative analysis of heparin co-infusion. Mol. Ther. *5*, 371–380.

11. Summerford, C., and Samulski, R.J. (1998). Membrane-associated heparan sulfate proteoglycan is a receptor for adeno-associated virus type 2 virions. J. Virol. *72*, 1438–1445.

12. Burger, C., Gorbatyuk, O.S., Velardo, M.J., Peden, C.S., Williams, P., Zolotukhin, S., Reier, P.J., Mandel, R.J., and Muzyczka, N. (2004). Recombinant AAV viral vectors pseudotyped with viral capsids from serotypes 1, 2, and 5 display differential efficiency and cell tropism after delivery to different regions of the central nervous system. Mol. Ther. *10*, 302–317.

13. Pillay, S., Meyer, N.L., Puschnik, A.S., Davulcu, O., Diep, J., Ishikawa, Y., Jae, L.T., Wosen, J.E., Nagamine, C.M., Chapman, M.S., and Carette, J.E. (2016). An essential receptor for adeno-associated virus infection. Nature *530*, 108–112.

14. Cearley, C.N., and Wolfe, J.H. (2006). Transduction characteristics of adeno-associated virus vectors expressing cap serotypes 7, 8, 9, and Rh10 in the mouse brain. Mol. Ther. *13*, 528–537.

15. Taymans, J.-M., Vandenberghe, L.H., Haute, C.V.D., Thiry, I., Deroose, C.M., Mortelmans, L., Wilson, J.M., Debyser, Z., and Baekelandt, V. (2007). Comparative analysis of adeno-associated viral vector serotypes 1, 2, 5, 7, and 8 in mouse brain. Hum. Gene Ther. *18*, 195–206.

16. Kells, A.P., Hadaczek, P., Yin, D., Bringas, J., Varenika, V., Forsayeth, J., and Bankiewicz, K.S. (2009). Efficient gene therapy-based method for the delivery of therapeutics to primate cortex. Proc. Natl. Acad. Sci. USA *106*, 2407–2411.

17. Pomin, V.H., and Mulloy, B. (2015). Current structural biology of the heparin interactome. Curr. Opin. Struct. Biol. *34*, 17–25.

18. Hamilton, J.F., Morrison, P.F., Chen, M.Y., Harvey-White, J., Pernaute, R.S., Phillips, H., Oldfield, E., and Bankiewicz, K.S. (2001). Heparin coinfusion during convection-enhanced delivery (CED) increases the distribution of the glial-derived neurotrophic factor (GDNF) ligand family in rat striatum and enhances the pharmacological activity of neurturin. Exp. Neurol. *168*, 155–161.

19. Hadaczek, P., Mirek, H., Bringas, J., Cunningham, J., and Bankiewicz, K. (2004). Basic fibroblast growth factor enhances transduction, distribution, and axonal transport of adeno-associated virus type 2 vector in rat brain. Hum. Gene Ther. *15*, 469–479.

20. Sullivan, J.A., Stanek, L.M., Lukason, M.J., Bu, J., Osmond, S.R., Barry, E.A., O'Riordan, C.R., Shihabuddin, L.S., Cheng, S.H., and Scaria, A. (2018). Rationally designed AAV2 and AAVrh8R capsids provide improved transduction in the retina and brain. Gene Ther. *25*, 205–219.

21. Hadaczek, P., Stanek, L., Ciesielska, A., Sudhakar, V., Samaranch, L., Pivirotto, P., Bringas, J., O'Riordan, C., Mastis, B., San Sebastian, W., et al. (2016). Widespread AAV1- and AAV2-mediated transgene expression in the nonhuman primate brain: implications for Huntington's disease. Mol. Ther. Methods Clin. Dev. *3*, 16037.

22. Kanaan, N.M., Sellnow, R.C., Boye, S.L., Coberly, B., Bennett, A., Agbandje-McKenna, M., Sortwell, C.E., Hauswirth, W.W., Boye, S.E., and Manfredsson, F.P. (2017). Rationally engineered AAV capsids improve transduction and volumetric spread in the CNS. Mol. Ther. Nucleic Acids *8*, 184–197.

23. Hordeaux, J., Wang, Q., Katz, N., Buza, E.L., Bell, P., and Wilson, J.M. (2018). The neurotropic properties of AAV-PHP.B are limited to C57BL/6J mice. Mol. Ther. *26*, 664–668.

24. San Sebastian, W., Kells, A.P., Bringas, J., Samaranch, L., Hadaczek, P., Ciesielska, A., Macayan, M., Pivirotto, P.J., Forsayeth, J., Osborne, S., et al. (2014). Safety and tolerability of MRI-guided infusion of AAV2-hAADC into the mid-brain of non-human primate. Mol. Ther. Methods Clin. Dev. *3*, e14049.

25. Mandel, R.J., Marmion, D.J., Kirik, D., Chu, Y., Heindel, C., McCown, T., Gray, S.J., and Kordower, J.H. (2017). Novel oligodendroglial alpha synuclein viral vector models of multiple system atrophy: studies in rodents and nonhuman primates. Acta Neuropathol. Commun. *5*, 47.

26. Ciesielska, A., Hadaczek, P., Mittermeyer, G., Zhou, S., Wright, J.F., Bankiewicz, K.S., and Forsayeth, J. (2013). Cerebral infusion of AAV9 vector-encoding non-self proteins can elicit cell-mediated immune responses. Mol. Ther. *21*, 158–166.

27. Forsayeth, J., and Bankiewicz, K.S. (2015). Transduction of antigen-presenting cells in the brain by AAV9 warrants caution in preclinical studies. Mol. Ther. *23*, 612.

28. Samaranch, L., Sebastian, W.S., Kells, A.P., Salegio, E.A., Heller, G., Bringas, J.R., Pivirotto, P., DeArmond, S., Forsayeth, J., and Bankiewicz, K.S. (2014). AAV9-mediated expression of a non-self protein in nonhuman primate central nervous system triggers widespread neuroinflammation driven by antigen-presenting cell transduction. Mol. Ther. *22*, 329–337.

29. Samaranch, L., Salegio, E.A., San Sebastian, W., Kells, A.P., Bringas, J.R., Forsayeth, J., and Bankiewicz, K.S. (2013). Strong cortical and spinal cord transduction after AAV7 and AAV9 delivery into the cerebrospinal fluid of nonhuman primates. Hum. Gene Ther. *24*, 526–532.

30. Hadaczek, P., Forsayeth, J., Mirek, H., Munson, K., Bringas, J., Pivirotto, P., McBride, J.L., Davidson, B.L., and Bankiewicz, K.S. (2009). Transduction of nonhuman primate brain with adeno-associated virus serotype 1: vector trafficking and immune response. Hum. Gene Ther. *20*, 225–237.

31. Foust, K.D., Nurre, E., Montgomery, C.L., Hernandez, A., Chan, C.M., and Kaspar, B.K. (2009). Intravascular AAV9 preferentially targets neonatal neurons and adult astrocytes. Nat. Biotechnol. *27*, 59–65.

32. Szuchet, S., Nielsen, J.A., Lovas, G., Domowicz, M.S., de Velasco, J.M., Maric, D., and Hudson, L.D. (2011). The genetic signature of perineuronal oligodendrocytes reveals their unique phenotype. Eur. J. Neurosci. *34*, 1906–1922.

33. Qing, K., Mah, C., Hansen, J., Zhou, S., Dwarki, V., and Srivastava, A. (1999). Human fibroblast growth factor receptor 1 is a co-receptor for infection by adeno-associated virus 2. Nat. Med. *5*, 71–77.

34. Chen, H., McCarty, D.M., Bruce, A.T., Suzuki, K., and Suzuki, K. (1998). Gene transfer and expression in oligodendrocytes under the control of myelin basic protein transcriptional control region mediated by adeno-associated virus. Gene Ther. *5*, 50–58.

35. Lawlor, P.A., Bland, R.J., Mouravlev, A., Young, D., and During, M.J. (2009). Efficient gene delivery and selective transduction of glial cells in the mammalian brain by AAV serotypes isolated from nonhuman primates. Mol. Ther. *17*, 1692–1702.

36. Powell, S.K., Khan, N., Parker, C.L., Samulski, R.J., Matsushima, G., Gray, S.J., and McCown, T.J. (2016). Characterization of a novel adeno-associated viral vector with preferential oligodendrocyte tropism. Gene Ther. *23*, 807–814.

37. Green, F., Samaranch, L., Zhang, H.S., Manning-Bog, A., Meyer, K., Forsayeth, J., and Bankiewicz, K.S. (2016). Axonal transport of AAV9 in nonhuman primate brain. Gene Ther. *23*, 520–526.

38. Samaranch, L., Blits, B., San Sebastian, W., Hadaczek, P., Bringas, J., Sudhakar, V., Macayan, M., Pivirotto, P.J., Petry, H., and Bankiewicz, K.S. (2017). MR-guided parenchymal delivery of adeno-associated viral vector serotype 5 in non-human primate brain. Gene Ther. *24*, 253–261.

39. Davidson, B.L., Stein, C.S., Heth, J.A., Martins, I., Kotin, R.M., Derksen, T.A., Zabner, J., Ghodsi, A., and Chiorini, J.A. (2000). Recombinant adeno-associated virus type 2, 4, and 5 vectors: transduction of variant cell types and regions in the mammalian central nervous system. Proc. Natl. Acad. Sci. USA *97*, 3428–3432.

40. McCown, T.J., Xiao, X., Li, J., Breese, G.R., and Samulski, R.J. (1996). Differential and persistent expression patterns of CNS gene transfer by an adeno-associated virus (AAV) vector. Brain Res. *713*, 99–107.

41. Lo, W.D., Qu, G., Sferra, T.J., Clark, R., Chen, R., and Johnson, P.R. (1999). Adeno-associated virus-mediated gene transfer to the brain: duration and modulation of expression. Hum. Gene Ther. *10*, 201–213.

42. Deverman, B.E., Pravdo, P.L., Simpson, B.P., Kumar, S.R., Chan, K.Y., Banerjee, A., Wu, W.L., Yang, B., Huber, N., Pasca, S.P., and Gradinaru, V. (2016). Cre-dependent selection yields AAV variants for widespread gene transfer to the adult brain. Nat. Biotechnol. *34*, 204–209.

43. Samaranch, L., Sebastian, W.S., Kells, A.P., Salegio, E.A., Heller, G., Bringas, J.R., Pivirotto, P., DeArmond, S., Forsayeth, J., and Bankiewicz, K.S. (2014). AAV9-mediated expression of a non-self protein in nonhuman primate central nervous system triggers widespread neuroinflammation driven by antigen-presenting cell transduction. Mol. Ther. *22*, 329–337.

44. Opie, S.R., Warrington, K.H., Jr., Agbandje-McKenna, M., Zolotukhin, S., and Muzyczka, N. (2003). Identification of amino acid residues in the capsid proteins of adeno-associated virus type 2 that contribute to heparan sulfate proteoglycan binding. J. Virol. *77*, 6995–7006.

45. Xiao, X., Li, J., and Samulski, R.J. (1998). Production of high-titer recombinant adeno-associated virus vectors in the absence of helper adenovirus. J. Virol. *72*, 2224–2232.

46. Nass, S.A., Mattingly, M.A., Woodcock, D.A., Burnham, B.L., Ardinger, J.A., Osmond, S.E., Frederick, A.M., Scaria, A., Cheng, S.H., and O'Riordan, C.R. (2017). Universal method for the purification of recombinant AAV vectors of differing serotypes. Mol. Ther. Methods Clin. Dev. *9*, 33–46.

47. Burnham, B., Nass, S., Kong, E., Mattingly, M., Woodcock, D., Song, A., Wadsworth, S., Cheng, S.H., Scaria, A., and O'Riordan, C.R. (2015). Analytical ultracentrifugation as an approach to characterize recombinant adeno-associated viral vectors. Hum. Gene Ther. Methods *26*, 228–242.

48. Nguyen, J.B., Sánchez-Pernaute, R., Cunningham, J., and Bankiewicz, K.S. (2001). Convection-enhanced delivery of AAV-2 combined with heparin increases TK gene transfer in the rat brain. Neuroreport *12*, 1961–1964.

49. Fiandaca, M.S., Forsayeth, J.R., Dickinson, P.J., and Bankiewicz, K.S. (2008). Image-guided convection-enhanced delivery platform in the treatment of neurological diseases. Neurotherapeutics *5*, 123–127.

50. Su, X., Kells, A.P., Salegio, E.A., Richardson, R.M., Hadaczek, P., Beyer, J., Bringas, J., Pivirotto, P., Forsayeth, J., and Bankiewicz, K.S. (2010). Real-time MR imaging with Gadoteridol predicts distribution of transgenes after convection-enhanced delivery of AAV2 vectors. Mol. Ther. *18*, 1490–1495.

51. Bankiewicz, K.S., Sudhakar, V., Samaranch, L., San Sebastian, W., Bringas, J., and Forsayeth, J. (2016). AAV viral vector delivery to the brain by shape-conforming MR-guided infusions. J. Control. Release *240*, 434–442.

52. Samaranch, L., Salegio, E.A., San Sebastian, W., Kells, A.P., Foust, K.D., Bringas, J.R., Lamarre, C., Forsayeth, J., Kaspar, B.K., and Bankiewicz, K.S. (2012). Adeno-associated virus serotype 9 transduction in the central nervous system of nonhuman primates. Hum. Gene Ther. *23*, 382–389.